Spectral tuning of a broadband optical pulse via stimulated Raman scattering of a prealigned molecule

Yunlong Mo [1], Wei Cao [1,*] Zegui Wang,[1] Xuechun Sun,[1] Qingbin Zhang,[1] and Peixiang Lu[1,2,†]

[1]*School of Physics and Wuhan National Laboratory for Optoelectronics,*
Huazhong University of Science and Technology, Wuhan 430074, China
[2]*Optics Valley Laboratory, Wuhan 430074, China*

The nonlinear spectral broadening of a near-infrared laser pulse propagating through pre-aligned molecules is investigated experimentally in a pump-probe scheme. The spectral shift of over 100 nm as well as spectral shaping is achieved via tuning the experimental conditions such as pump-probe delay, gas pressure, and pulse energy. Numerical simulation based on the nonlinear Schrödinger equation shows that the experimentally observed spectral tuning is due to the competition between different nonlinear effects, i.e., stimulated Raman scattering, the Kerr effect, and molecular alignment. Adjusting the pump-probe delay properly can decouple different nonlinear processes and allows for spectral tuning in a controlled way. This scheme is demonstrated to be attractive for the generation of few-cycle laser pulses with a frequency-tunable spectrum, broadband pulse shaping, and many strong field applications in the visible range.

I. INTRODUCTION

Nowadays, the exploration of light-matter interactions under shorter and shorter timescales and high-intensities has promoted the development of ultra-short laser sources, especially few-cycle laser pulses with frequency tunability over a broad spectral range, which have a wide range of applications in attosecond physics [1–3], chemical reaction dynamics [4–6], and high time-resolution measurements in atomic and molecular physics [7], as well as molecular alignment [8].

Optical parametric amplification (OPA) and optical parametric chirped pulse amplification (OPCPA) are well-established technologies for producing frequency-tunable laser pulses [9–11]. The efficiency of the entire nonlinear process is limited due to the rigorous condition of the precise phase matching over a broad spectrum. Filamentation in rare gases and hollow core fiber (HCF) filled with rare gases could also achieve spectral shift by self-phase modulation (SPM) and self-steepening [12–15]. Supercontinuum generation is also realized by four-wave mixing process with cascaded Raman scattering in microstructured fibers [16–22]. Recently, owing to the enhanced spectral broadening caused by the delayed rotational nonlinearity, molecular gas was proposed as an alternative to rare gas to obtain a larger frequency shift and larger compression factors with long input pulse duration in HCF. Safaei *et al.* [23] reported the observation of the formation of highly stable multidimensional solitary states (MDSS) in HCF filled with molecular gases and found the generation of a broadband red-shifted spectrum and an unusual

negative second-order spectral phase due to the enhanced Raman processes caused by the intermodal interactions. Beetar *et al.* [24], Fan *et al.* [25], and Carpeggiani *et al.* [26] also demonstrated the generation of supercontinuum infrared spectrum in the long-distance HCFs filled with molecular gases with high conversion efficiency and high beam quality. In all these methods a few hundred femtosecond single pulse is used to simultaneously launch the rotation wave packet in the leading edge, and accumulate a time-dependent nonlinear phase in the falling edge causing the spectral broadening. Such spectral tuning scheme will have extended applications if the molecular alignment and spectral broadening are controllable separately with a pump-probe manner.

Specifically, molecules can be prealigned as a substitute for noble gas media in nonlinear interaction, which opens up many important applications in ultrafast optics, particularly the structure and length of the filament [27,28], shock x waves [29–31], terahertz (THz) waves [32–36], and high harmonic generation (HHG) [37,38]. Most of the previous works were performed in free-space rather than in the HCF. Similarly, the frequency shift by molecular phase modulation (MPM) in filaments and HCFs was shown theoretically in pump-probe schemes [39–42]. Zhavoronkov *et al.* [43], Bartels *et al.* [44], and Noack *et al.* [45] experimentally demonstrated the modulation and compression of pulses in the ultraviolet (UV) region by using a Raman active media based on waveguide, where an 800-nm pump pulse is used to excite molecules and change the refractive index of the gas, then a time-delayed 400-nm UV probe pulse is used to sense the molecular alignment revivals. Further, increasing the bandwidth of the probe pulse indicates an enhanced Raman scattering, which is challenging due to the group velocity mismatch between the near-infrared range (NIR) pump and UV probe propagating in the long waveguide [46,47].

*weicao@hust.edu.cn
†lupeixiang@mail.hust.edu.cn

Cai *et al.* [48,49] experimentally showed that a super-continuum pulse can be generated through femtosecond filamentation in prealigned diatomic molecules in the visible region, this configuration avoids the group velocity mismatching problem by using similar wavelength for both the pump pulse and probe pulse, yet the spectral tuning range is limited by the relatively short filament length. Combining the pump-probe configuration with similar wavelength and a HCF holds the promise to overcome the mentioned issues thanks to the longer nonlinear action length, reduced group velocity mismatch, and higher transmission efficiency as compared with filamentation.

In this study, we experimentally demonstrated the spectral broadening of a laser pulse in the NIR in a HCF filled with prealigned nitrogen and nitrous oxide. We find that not only the central frequency, but also the spectral shape of the probe pulse can be tuned to a large extend by optimizing different experimental parameters based on molecular phase modulation in our pump-probe scheme. A theoretical model incorporating different nonlinear effects including the Kerr effect, molecular alignment, and SRS is utilized to analyze the nonlinear interactions, and the experimental observations are well explained by our theoretical simulation. This scheme has great potential for ultra-wide range spectral tuning from UV to midinfrared.

II. EXPERIMENTAL RESULTS

The experimental apparatus is shown in Fig. 1(a) in our studies. An 800-nm 30-fs femtosecond pulse provided by a 1 kHz Ti:sapphire amplified laser system is first split by a beam splitter (BS1) into a pump pulse for molecular pre-alignment and a probe pulse for investigating its propagation dynamics. The pulses are then recombined and collinearly focused with a concave mirror (M8, focal length of 2 m) into a 1-m HCF filled with molecular gas. The polarization direction of the pump pulse is perpendicular to that of the probe pulse by rotating the half-wave plate (HWP) in the pump arm before the recombination mirror (BS2). The relative delay between the pump pulse and the probe pulse is adjusted by using a motorized translation stage with a delay step of 1.5 μm. At the exit of the HCF, the spectrum of the probe pulse, which is collimated by the other concave mirror (M9, focal length of 2 m), is measured by the spectrometer after a polarizer which reflected the *s*-polarized pump pulse and transmitted the *p*-polarized probe pulse. All experiments are performed at room temperature.

Figure 1(b) shows the delay-dependent spectrum of a 0.12-mJ probe pulse propagating through a 1-m HCF filled with 1.8 bar nitrogen aligned by 0.41-mJ pump pulse. The periodic modulation on the spectrum of the probe pulse is a clear indication of molecular rotational wave packet launched by the pump pulse. The four special revivals of nitrogen molecular alignment are marked with $1/4T_{\text{rev}\_N2}$, $1/2T_{\text{rev}\_N2}$, $3/4T_{\text{rev}\_N2}$, and T_{rev_N2} in Fig. 1(b), respectively, where T_{rev_N2} represents the revival period of nitrogen molecular alignment. In addition, the corresponding revival time is 8.4 ps, which is consistent with previous works [44,50,51]. At the same time, the spectrum of the probe pulse is broadened or narrowed at certain delays, corresponding to the polarization
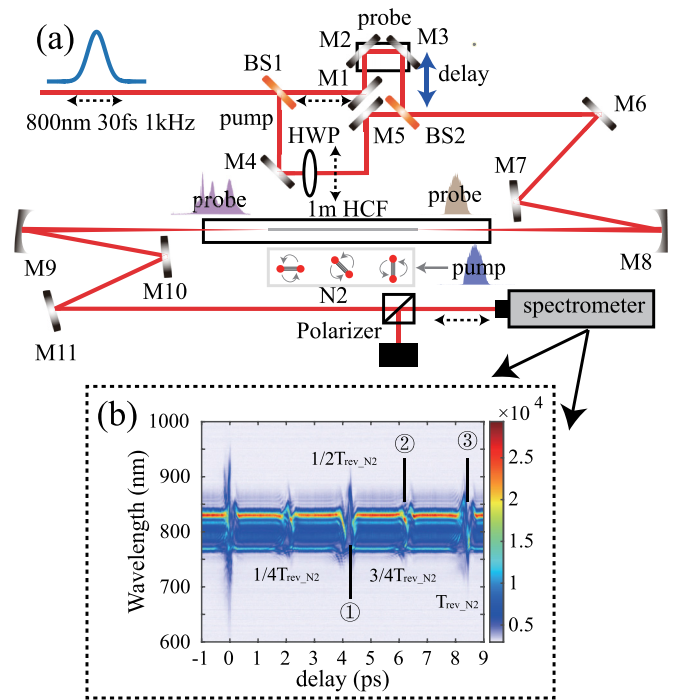
FIG. 1. (a) Experimental layout: BS1, BS2, beam splitter; HWP, half-wave plate; M1-M7, M10, M11, high reflectivity mirror with broadband; M8, M9, concave mirror with focal length of 2 m; Polarizer, reflect the *s*-polarized pump and transmit the *p*-polarized probe; motorized translation stage, control the relative delay between pump pulse and probe pulse with a delay step of 1.5 μm. Panel (b) depicts the spectrum of 0.12 mJ probe pulse propagating in a 1m HCF filled with 1.8 bar nitrogen excited by 0.41 mJ pump pulse at different delays. The dashed lines with arrows indicate the polarization directions of the pulses.

direction of the probe pulse perpendicular or parallel to the prealigned molecular axis [48]. It also can be seen that the delay-dependent spectrum of the probe pulse has an overall redshift compared with [52,53], and the main energy is concentrated around 830 nm. The more complicated spectral profile close-to-zero delay is caused by direct cross-phase modulation of the pump and probe pulses. Meanwhile, it is measured that the spatial profile of the probe pulse remains constant and the beam has good stability.

To inspect the spectral tuning capability of the current scheme in more details we choose three specific delays near 1/2, 3/4, and full revival time to study the spectrum of the probe pulse at different pressures as shown in Fig. 2. The positions of the three delays are marked by the numbers in Fig. 1(b). As can be seen from Fig. 2(a), compared with the spectrum of the input probe pulse (gray shades), the spectrum of the output probe pulse exhibits obvious red shift (4.28 ps), blue shift (8.41 ps), and symmetrical broadening even spectrum shaping (6.21 ps) at different delays under fixed pressure. These phenomena indicate that the spectral tuning of the probe pulse can be preliminarily achieved by simply adjusting the relative delay between the probe pulse and the pump pulse. It can be seen that the spectrum of the probe pulse at different gas pressures experiences a different amount of shift and broadening from Figs. 2(b) to 2(d). As the pressure
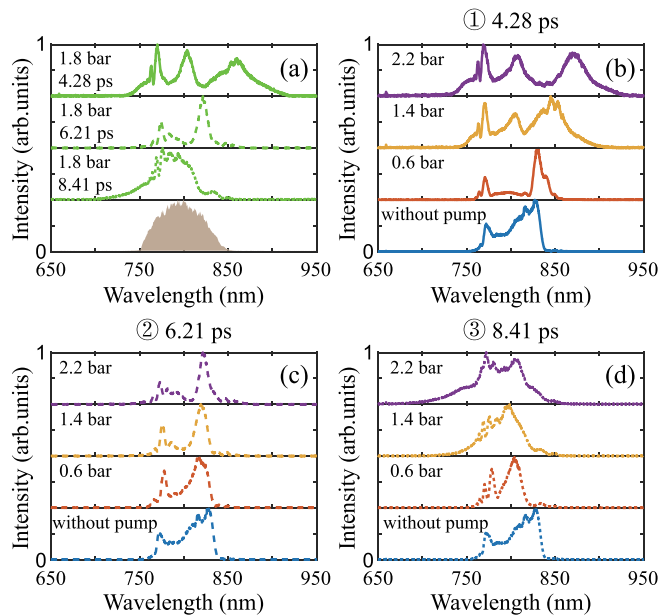
FIG. 2. Panel (a) represents the spectrum of the probe pulse at three different delays (4.28 ps, 6.21 ps, 8.41 ps) in Fig. 1(b) and the spectrum of the input probe pulse (gray shades). The spectrum of the probe pulse at various pressures (0.6 bar, 1.4 bar, 2.2 bar) for the delay of (b) 4.28 ps (solid line), (c) 6.21 ps (dashed line), (d) 8.41 ps (dotted line) based on Fig. 1(b). The blue lines represent the spectrum of the probe pulse without the pump pulse at 0.6 bar.

FIG. 3. Panel (a) represents the spectrum of the probe pulse propagating in a 1 m HCF filled with 1.8 bar nitrogen excited by 0.5 mJ pump pulse at different delays. The spectrum of the probe pulse at delays (3.45 ps, 4.17 ps, 4.26 ps, 4.35 ps) near the half revival of the rotational wave packet show in (b). The spectrum of the probe pulse at various pressures (0.6 bar, 1.4 bar, 2.2 bar) for the delay of (c) 4.28 ps (solid line), (d) 8.41 ps (dotted line) based on (a). The blue lines represent the spectrum of the probe pulse without the pump pulse at 0.6 bar.

increases, the amount of spectral shift and broadening is also increasing monotonically for all three delays. The spectra of the probe pulse at more pressures are shown in Appendix B. This is different from the spectral broadening from SPM in atomic gases, where the generation of new frequencies below and above the fundamental frequency occurs at the leading and trailing edges of the pulse resulting in a symmetrical spectrum [24,54].

It is worth mentioning that we can control not only the shift and broadening, but also the spectral shape of the probe pulse, which is very attractive for the shaping of the broadband spectrum. It is shown that the shape of the spectrum will gradually change as the gas pressure increases in Figs. 2(b) to 2(d). In particular, with the increase of gas pressure, the spectral modulation depth accompanied by spectral blueshift becomes shallower in Fig. 2(d), but the spectral modulation depth of the probe pulse without obvious spectral broadening becomes larger in Fig. 2(c). These observations hint at a potential scheme for spectral broadening and shaping with great tunability.

The spectrum of 0.12-mJ probe pulse propagating in a 1-m HCF filled with 1.8 bar nitrogen excited by a higher-energy pump pulse (0.50 mJ) is also investigated and shown in Fig. 3(a). Figure 3(b) depicts the spectrum of the probe pulse at delays near the half revival of the rotational wave packet. Among them, the spectral intensities of the probe pulse of 3.45 ps, 4.17 ps, and 4.26 ps are relatively normalized with respect to that of 4.35 ps, respectively. The energy exchange between the electromagnetic field and the molecules during the nonlinear interaction depends on the polarization direction of the

electric field. When the polarization is parallel (perpendicular) to the molecular axis, the molecules lose (gain) energy to (from) the electric field [55,56]. At the same time, the energy increase and decrease of the probe pulse correspond to the blue-shift and red-shift of the spectrum of the probe pulse, respectively. Therefore, it can be seen from Fig. 3(b) that the frequency shift and broadening of the spectrum of the probe pulse are accompanied by energy changes. The spectrum of the probe pulse for higher-energy pump pulse under various pressures is shown in Figs. 3(c) and 3(d). It can be found that in the case of high-energy pump pulse, the spectrum of the probe pulse achieves a larger redshift (blueshift) of about 100 nm at 4.28 ps (8.41 ps). Similarly, the variation trend of spectral modulation depth with gas pressure is consistent for different pump energies. Therefore, the spectral tuning of the broadband optical pulse can be optimized by controlling pump-probe delay, the energy of the pulse, and gas pressure in HCF.

Under similar experimental conditions, nitrous oxide is also investigated to further study, to a greater extent, the spectral shift and modulation of the probe pulse. The nonlinear refractive index and instantaneous frequency shift of nitrous oxide are much larger than those of nitrogen, as demonstrated in [24,53], so the use of nitrous oxide in HCFs holds promise for a wider range of spectral tuning. The delay-dependent spectrum of a 0.07-mJ probe pulse propagating in the HCF filled with 1 bar nitrous oxide aligned by a 0.15-mJ pump pulse is also shown in Fig. 4(a). Obviously, compared with the results of nitrogen, the spectrum of the probe pulse has weaker blueshift but more obvious redshift in the prealigned nitrous oxide [24], and the 1/4 and 3/4 revivals are not present owing
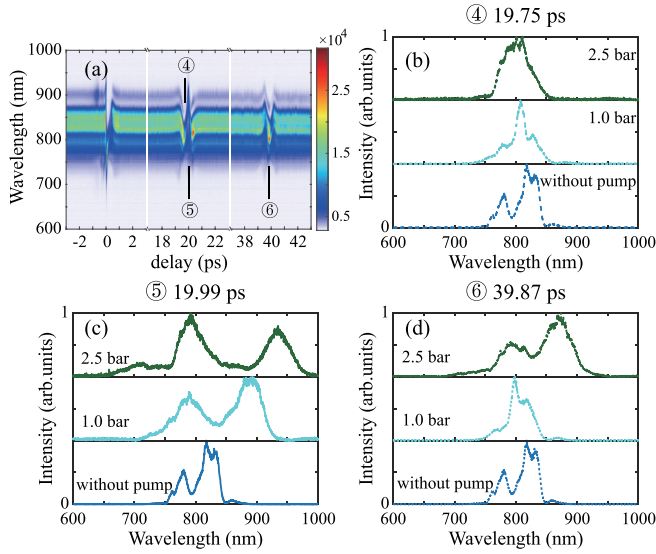
FIG. 4. Panel (a) represents the spectrum of 0.07-mJ probe pulse propagating in a 1-m HCF filled with 1 bar nitrous oxide excited by the pump pulse with 0.15 mJ at different delays. The spectrum of the probe pulse at various pressures (1 bar, 2.5 bar) for the delay of (b) 19.75 ps (dashed line), (c) 19.99 ps (solid line), (d) 39.87 ps (dotted line) based on (a). The blue lines represent the spectrum of the probe pulse without the pump pulse at 1 bar.

to the axial asymmetry of the linear N_2O molecule, in which the atoms are ordered N-N-O [53]. In Fig. 4(a), the spectrum of the probe pulse also demonstrates the energy loss, energy gain, and different amount of spectral modulation of the probe pulse in pr-aligned nitrous oxide near the half and full revival times. The effect of different gas pressures on the spectrum of the probe pulse is further studied under three special delays (19.75 ps, 19.99 ps, 39.87 ps), depicted in Figs. 4(b) to 4(d). The results show that, as the pressure increases, the spectrum of the probe pulse will be further redshifted, blueshifted, and symmetrically broadened, respectively, and the redshift amount has been extended to 150 nm. It can be seen that the systematic variation of the spectral shape of the probe pulse, i.e., the change of the spectral modulation depth with the gas pressure is consistent with the results of nitrogen.

III. THEORETICAL ANALYSIS

To illustrate how the dynamics of the different nonlinearity affect the generated tunable broadband spectrum, we calculate the spectrum generated from propagation of the probe pulse in HCF filled with prealigned molecular gas. The pulse propagation equation can be written as [52,57]

$$\frac{\partial \varepsilon}{\partial z} = \frac{i}{2k}\left(\frac{\partial^2}{\partial x^2} + \frac{\partial^2}{\partial y^2}\right)\varepsilon - \frac{ik''}{2}\frac{\partial^2 \varepsilon}{\partial t^2} + N(|\varepsilon|^2, \rho)\varepsilon - \frac{\alpha}{2}\varepsilon, \tag{1}$$

where

$$N(|\varepsilon|^2, \rho) = N_{\text{Kerr}}(|\varepsilon|^2) + N_{\text{SRS}}(|\varepsilon|^2) + N_{\text{Plasma}}(\rho)$$
$$+ N_{\text{MPA}}(|\varepsilon|^2) + N_{\text{Align}}(\ll \cos^2 \theta \gg), \tag{2}$$

where ε represents the probe-pulse field envelope and N is the nonlinear effect that the probe pulse experienced in HCF,
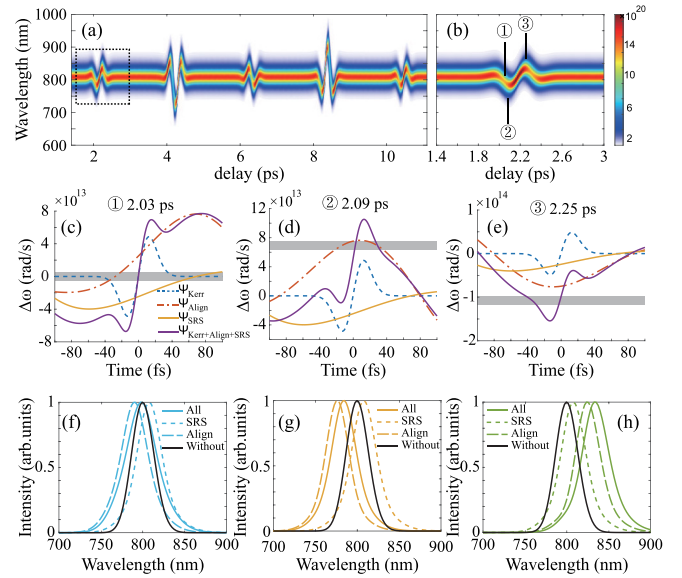
FIG. 5. Panel (a) represents the delay-dependent spectrum of the probe pulse E_1 propagating in a 1-m HCF filled with 1 bar nitrogen excited by the pump pulse E_2 at 25°C. Panel (b) is the part of (a), which is shown in the dotted box in (a) The frequency shift $\Delta\omega = -\partial\psi/\partial t$ caused by different nonlinear effects for the delay of (c) 2.03 ps, (d) 2.09 ps, and (e) 2.25 ps based on (a). Shaded area shows the average value of frequency shift of the probe pulse. The spectrum of the probe pulse with only SRS, only molecular alignment and all nonlinear effects for the delay of (f) 2.03 ps, (g) 2.09 ps, and (h) 2.25 ps based on (a).

including the Kerr effect (N_{Kerr}), SRS (N_{SRS}), plasma term (N_{Plasma}), multiphoton absorption (N_{MPA}), and nonlinearity induced by molecular alignment (N_{Align}). The details of the theoretical model are given in the Appendix.

In our simulation, the spatial profile of the beam remains constant due to the low input energy. The electric field form of the input probe pulse is $E_1(t) = \varepsilon_1 \exp(i\omega_0 t)$, $\varepsilon_1 = \sqrt{I_1}\exp(-2\ln 2 t^2/\tau_1^2)$, the pump pulse is $E_2(t) = \varepsilon_2 \exp(i\omega_0 t)$, $\varepsilon_2 = \sqrt{I_2}\exp(-2\ln 2 t^2/\tau_2^2)$, with the same polarization direction as E_1. $I_1 = 5.90 \times 10^{12}$ W/cm^2 and $I_2 = 1.18 \times 10^{13}$ W/cm^2 represent the intensity of the probe pulse and the pump pulse, respectively, $\tau_1 = \tau_2 = 30$ fs is the pulse full width at half maximum (FWHM). $\omega_0 = 2\pi c/\lambda$ is the central frequency with $\lambda = 800$ nm and $c = 3 \times 10^8$ m/s.

Before the interaction, the gas ensemble is assumed to be in a thermal equilibrium state with a Boltzmann distribution at temperature 25°C. First, we calculated the transmitted spectrum of the probe pulse in a 1-m HCF filled with 1 bar nitrogen under different delays between the pump and probe, and the results are shown in Figs. 5(a) and 5(b). It can be clearly seen that the spectrum of the probe pulse has different degrees of frequency shift at different delays and the overall characteristics of the spectrogram are consistent with the experiment shown in Figs. 1(b) and 3(a). It should be noted that, in the one-dimensional simulation, the polarization of the probe is parallel to that of the pump pulse, thus the calculated revival dynamics is opposite to that of the measurement in Fig. 1(b). However, the polarization of the probe pulse does not influence the characteristic feature of the broadened spectrum. It

is crucial for us to be able to distinguish different nonlinear effects to achieve more reliable control for pulses bearing broad bandwidth in our pump-probe scheme. So we select three specific delays 2.03 ps, 2.09 ps, and 2.25 ps for further analysis. The phase ψ accumulated by different nonlinear effects in HCF can be calculated $\psi = N_{\text{nonlinear effect}} L$, where L is the length of the HCF. The frequency shift $\Delta\omega$ can be obtained by taking the time derivative of the accumulated phase ψ for different nonlinear effects, as shown in Figs. 5(c) to 5(e). The blue dotted line, orange dot-and-dash line, and yellow solid line represent the frequency shift caused by the Kerr effect, molecular alignment, and SRS in the HCF, respectively. In addition, the purple solid line is the sum of all the nonlinear effects. Meanwhile, the average values of the overall frequency shift are shown in the shaded areas in Figs. 5(c) to 5(e) at different delays.

Figures 5(f) to 5(h) show the calculated spectrum of the probe pulse when only SRS, only molecular alignment, or all nonlinear effects are considered, and the black solid line represents the spectrum of the probe pulse at the entrance of the HCF. It can be found that the total frequency shift of the probe pulse is close to zero at 2.03 ps [Fig. 5(c)], where the Kerr effect plays a major role, and the frequency shift caused by the SRS effect and the molecular alignment cancel each other out, therefore the spectrum of the probe pulse is symmetrically broadened along both sides of the center wavelength [Fig. 5(f)]. Also the total frequency shift of the probe pulse at 2.09 ps is greater than zero [Fig. 5(d)], where the frequency shift caused by molecular alignment is larger than that caused by other nonlinearities, so the spectral blueshift of the probe pulse will occur [(Fig. 5(g)]. The total frequency shift of the probe pulse is less than zero at a delay of 2.25 ps [Fig. 5(e)], where the frequency shift caused by molecular alignment and SRS is dominant, and the spectrum of the probe pulse will be redshifted [Fig. 5(h)]. This explains why the redshift amount of the probe pulse is greater than the blueshift amount of the probe pulse in our experimental results. However, the probe pulse appears redshifted at delays away from the molecular alignment revivals' structure due to the dominance of the SRS effect. It can be clearly shown from these simulations that the influence of different nonlinear effects on the probe pulse can be explicitly understood and controlled and it provides a valid means for desirable spectral tuning of broadband optical pulses.

To further analyze the situation of different experimental parameters, we also investigate the influence of different intensities [Figs. 6(a) to 6(c)] of the probe pulse and different gas pressures [Figs. 6(d) to 6(f)] on the spectrum of the probe pulse. The spectrum of the probe pulse still exhibits symmetric broadening with the increase of the intensity of the probe pulse and gas pressure due to the dominant Kerr effect at 2.03 ps, and the modulation of spectral shape at high intensity and pressure is also caused by the Kerr effect. For the delay of 2.09 ps, the influence of molecular alignment remains unchanged while the SRS effect is enhanced with the increase of the probe pulse intensity, resulting in an insignificant blueshift of the probe pulse. However, the effect of molecular alignment is more obvious than other nonlinearities with the increase of gas pressure, resulting in an obvious blueshift of the spectrum of the probe pulse. For the delay of 2.25ps, the SRS effect and
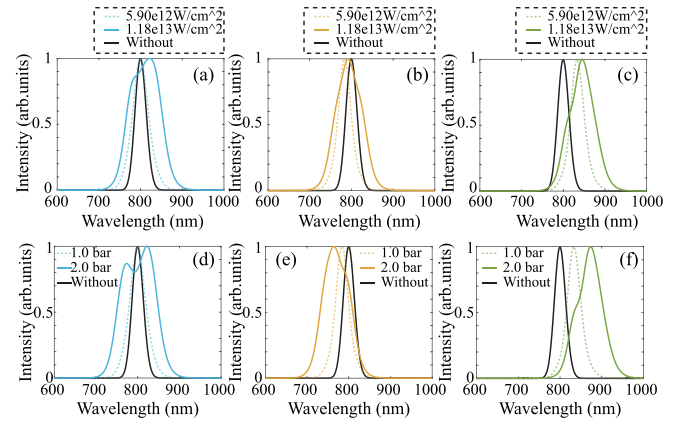
FIG. 6. The influence of the different intensities ($I_1 = 5.90 \times 10^{12}$ W/cm^2, $I_1 = 1.18 \times 10^{13}$ W/cm^2) of the probe pulse and different gas pressures (1 bar, 2 bar) on the spectral shift for the delay of (a,d) 2.03 ps, (b,e) 2.09 ps, and (c,f) 2.25 ps based on Fig. 5(a).

molecular alignment will be enhanced with the laser intensity and gas pressure because of the dominant role of both the SRS and molecular alignment, resulting in a more obvious redshift of the spectrum of the probe pulse. It is found that the spectrum of the probe pulse not only will be further shifted or broadened, but also has a slight change in spectral shape with the increase of gas pressure and intensity, which is consistent with the experimental observation. The main feature of the spectral modulation in Fig. 2 can be well reproduced in the simulation by assuming an input probe pulse with Gaussian envelope, the other effect such as the spectral splitting in Fig. 2 could be attributed to the more complex temporal structure of the input probe pulse. The theoretical analysis shows that different nonlinear effects can play a dominant role in the interaction with the appropriate parameters, so as to realize the control of the broadband spectrum. In addition, the variation trend of the spectrum of the probe pulse is in good agreement with experimental results.

The current study shows the tuning of a broadband pulse mainly in the VIS-NIR regime spanning from 600 to 1000 nm. A tunable midinfrared or ultraviolet spectrum can be achieved potentially by using a longer fiber ($\sim$6 m) with large inner diameter ($\sim$550 μm) and high-pressure ($\sim$6 bar) at lower temperature using the current scheme. To further increase the intensity of the pulse, a HCF with pressure gradient will be needed to effectively avoid the ionization that degrades the transmission efficiency and beam quality [58].

The spatial-temporal coupling effect must be considered in the theoretical analysis of the transmission process of high-energy probe pulses in a longer HCF with larger inner diameter and higher gas pressure. The coupling between different spatial modes will affect the contribution of different nonlinear effects and make the pulse propagation process more complicated [23,26]. The spectral tuning mechanism under such conditions deserves further study in the future.

IV. CONCLUSION

In conclusion, we experimentally investigated the spectral tuning of broadband optical pulses in the NIR range in a

HCF filled with prealigned nitrogen and nitrous oxide. Under a pump-probe scheme, the nonlinear interaction between the laser and the aligned molecules leads to large spectral shift of over 100 nm for proper pump-probe delays. At the same time, the spectral shape of the broadband optical pulse can be modulated by changing the experimental conditions such as the pump energies and gas pressure. The frequency shift, caused by different nonlinear effects, of the probe pulse are calculated, and the dominant roles of different nonlinear effects are identified under different conditions. There is good agreement between our theoretical simulations and experimental observations. It is demonstrated to be an effective approach for the generation of few-cycle laser pulses with frequency-tunable spectrum, which are significant for many strong-field applications. The current approach can be potentially extended for high-energy few-cycle laser pulse generation with desired spectrum using a HCF with larger inner diameter, longer distance, higher pressure, and lower temperature in the future.

ACKNOWLEDGMENTS

APPENDIX A: THEORETICAL MODEL

When molecules with anisotropic polarizability are excited by a pump pulse in a nonadiabatic alignment regime, the refractive index changes in time. The nonadiabatic molecular alignment induces periodic modulation of the refractive index of the gas. When the polarization direction of the probe pulse is the same as that of the pump pulse, the change of the refractive index of the molecular gas is expressed as [44,59]

$$\Delta n_{\parallel}(t) = \frac{2\pi \rho_{at}}{n_0} \Delta\alpha \left(\ll \cos^2\theta \gg (t) - \frac{1}{3} \right), \quad \text{(A1)}$$

where $(\ll \cos^2\theta \gg)$ is the expectation value of the thermally averaged alignment given by [60], ρ_{at} is the molecular density, and n_0 is the linear refractive index. $\Delta\alpha$ is the difference between the parallel $\alpha_{\parallel}$ and perpendicular $\alpha_{\perp}$ polarizability components with respect to the molecular axis and θ is the angle between the molecular axis and the polarization direction of the pump laser field. When the polarization direction of the probe pulse and the pump pulse is perpendicular to each other, the change of the refractive index of the molecular gas is

$$\Delta n_{\perp}(t) = -\frac{1}{2}\Delta n_{\parallel}(t) = -\frac{\pi \rho_{at}}{n_0} \Delta\alpha \left(\ll \cos^2\theta \gg (t) - \frac{1}{3} \right). \quad \text{(A2)}$$

The pulse propagation equation in HCF filled with prealigned molecular gas can be written as Eqs. (1) and (2), where

$$N_{\text{Kerr}}(|\varepsilon|^2) = ik_0 n_2 \hat{T}(1 - f_R)|\varepsilon|^2, \quad \text{(A3)}$$

$$N_{\text{SRS}}(|\varepsilon|^2) = ik_0 n_2 f_R \int_{-\infty}^{t} R(t-\tau)|\varepsilon|^2 d\tau, \quad \text{(A4)}$$

$$N_{\text{Plasma}}(\rho) = -\frac{\sigma}{2}(1 + i\omega_0\tau_c)\rho, \quad \text{(A5)}$$

$$N_{\text{MPA}}(|\varepsilon|^2) = -\frac{\beta_{\text{K}}}{2}|\varepsilon|^{2\text{K}-2}\left[1 - \frac{\rho}{\rho_{at}}\right], \quad \text{(A6)}$$

$$N_{\text{Align}}(\ll \cos^2\theta \gg) = ik_0 \hat{T} \Delta n, \quad \text{(A7)}$$

and

$$\frac{\partial \rho}{\partial t} = \eta \sigma_K |\varepsilon|^{2\text{K}}(\rho_{at} - \rho) + \frac{\sigma}{U_i}\rho|\varepsilon|^2, \quad \text{(A8)}$$

$$\sigma = \frac{k_0}{n_0 \rho_c} \frac{\omega_0 \tau_c}{1 + \omega_0^2 \tau_c^2}. \quad \text{(A9)}$$

Here ε represents the probe pulse field envelope and k is the wave vector. x and y describe the spatial coordinates of the probe pulse, N is the nonlinear effect that the probe pulse experienced in HCF, including the Kerr effect, plasma term, multiphoton absorption, and nonlinearity induced by molecular alignment. α is the absorption coefficient of the probe pulse in HCF. n_2 is the nonlinear refractive index, R is the Raman response function, f_R represents the fraction of the Raman nonlinearity in the overall nonlinear response of the fiber filled with molecular gas. k_0 and ω_0 are the central wave number and central frequency of the laser pulse. The operator $\hat{T}$ represents the self-steepening effect. ρ is the electron density, σ is the inverse bremsstrahlung cross section, and σ_K denotes the coefficient of the multiphoton ionization rate $W_{\text{MPI}} = \sigma_K I^K$ involving K photons, where $K \equiv < \frac{U_i}{\hbar\omega_0} + 1 >$, and U_i is the ionization potential of the molecular gas. The coefficient $\beta_K = K\hbar\omega_0\rho_{at}\sigma_K$ is related to the multiphoton ionization coefficient. The coefficient η given by [29] describes the dependence of ionization rate on molecular alignment. τ_c and ρ_c represent the electron collision time and the value of the critical plasma density above which the plasma becomes opaque, respectively.
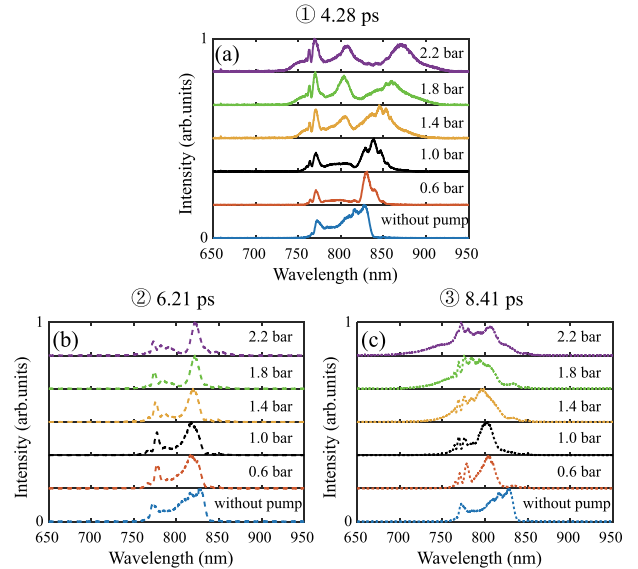
FIG. 7. The spectrum of the probe pulse at various pressures (0.6 bar, 1 bar, 1.4 bar, 1.8bar, 2.2 bar) for the delay of (a) 4.28 ps (solid line), (b) 6.21 ps (dashed line), and (c) 8.41 ps (dotted line) based on Fig. 1(b). The blue lines are the spectrum of the probe pulse without the pump pulse at 0.6 bar.
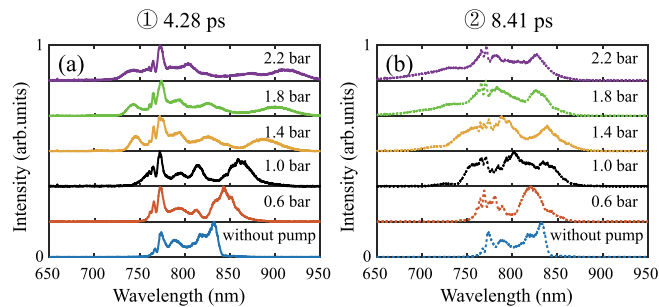
FIG. 8. The spectrum of the probe pulse at various pressures (0.6 bar, 1 bar, 1.4 bar, 1.8bar, 2.2 bar) for the delay of (a) 4.28 ps (solid line) and (b) 8.41 ps (dotted line) based on Fig. 3(a). The blue lines represent the spectrum of the probe pulse without the pump pulse at 0.6 bar.

APPENDIX B: COMPLETE EXPERIMENTAL DATA

Under the experimental parameters of Fig. 1(b), we studied the spectral shift degree and spectral shape of the probe pulse at three different delays (4.28 ps, 6.21 ps, 8.41 ps) under five pressures (0.6 bar, 1 bar, 1.4 bar, 1.8bar, 2.2 bar). Part of the results are shown in Fig. 2, and the complete results are shown in Fig. 7. With the increase of the pressure, both the spectral shift and the change regulation of the spectral shape of the probe pulse are consistent with the analysis in Fig. 2.

Similarly, the spectra of the probe pulse at two delays (4.28 ps, 8.41 ps) under five pressures (0.6 bar, 1 bar, 1.4 bar, 1.8bar, 2.2 bar) for the 0.5-mJ pump pulse are shown in Fig. 8, and some of the results are shown in Fig. 3. Figure 9 shows the spectrum of the probe pulse under four pressures (1 bar, 1.5 bar, 2 bar, 2.5 bar) with three different delays (19.75 ps, 19.99 ps, 39.87 ps) and the main conclusions are consistent
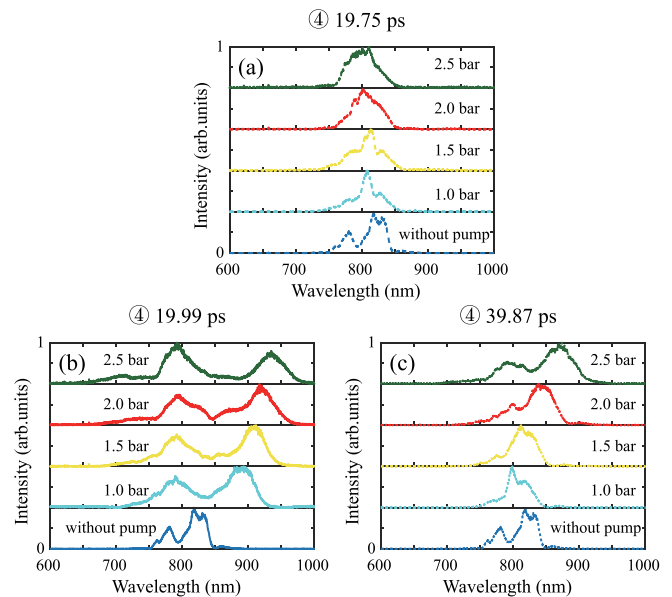
FIG. 9. The spectrum of the probe pulse at various pressures (1 bar, 1.5 bar, 2 bar, 2.5 bar) for the delay of (a) 19.75 ps (dashed line), (b) 19.99 ps (solid line), and (c) 39.87 ps (dotted line) based on Fig. 4(a). The blue lines represent the spectrum of the probe pulse without the pump pulse at 1 bar.

with the analysis results in Fig. 4. At the same time, it can be found that, as the gas pressure gradually increases, the change regulation of the spectral shape of the probe pulse is opposite to that of Fig. 7(b). Therefore, the spectral shape of broadband optical pulse can be realized by selecting different types of molecular gases, controlling the gas pressure, and selecting different pump-probe delays.

[1] N. Dudovich, O. Smirnova, J. Levesque, Y. Mairesse, M. Y. Ivanov, D. M. Villeneuve, and P. B. Corkum, Measuring and controlling the birth of attosecond XUV pulses, Nat. Phys. **2**, 781 (2006).

[2] F. Krausz and M. Ivanov, Attosecond physics, Rev. Mod. Phys. **81**, 163 (2009).

[3] C. Ott, A. Kaldun, L. Argenti, P. Raith, K. Meyer, M. Laux, Y. Zhang, A. Blättermann, S. Hagstotz, T. Ding, R. Heck, J. Madroñero, F. Martín, and T. Pfeifer, Reconstruction and control of a time-dependent two-electron wave packet, Nature (London) **516**, 374 (2014).

[4] M. Nisoli, P. Decleva, F. Calegari, A. Palacios, and F. Martín, Attosecond electron dynamics in molecules, Chem. Rev. **117**, 10760 (2017).

[5] I. V. Litvinyuk, K. F. Lee, P. W. Dooley, D. M. Rayner, D. M. Villeneuve, and P. B. Corkum, Alignment-Dependent Strong Field Ionization of Molecules, Phys. Rev. Lett. **90**, 233003 (2003).

[6] T. Suzuki, S. Minemoto, T. Kanai, and H. Sakai, Optimal Control of Multiphoton Ionization Processes in Aligned i₂ Molecules with Time-Dependent Polarization Pulses, Phys. Rev. Lett. **92**, 133005 (2004).

[7] Y. Liu, X. Liu, Y. Deng, C. Wu, H. Jiang, and Q. Gong, Selective Steering of Molecular Multiple Dissociative Channels with Strong Few-Cycle Laser Pulses, Phys. Rev. Lett. **106**, 073004 (2011).

[8] S. Varma, Y.-H. Chen, and H. M. Milchberg, Trapping and Destruction of Long-Range High-Intensity Optical Filaments by Molecular Quantum Wakes in Air, Phys. Rev. Lett. **101**, 205001 (2008).

[9] G. Cerullo and S. De Silvestri, Ultrafast optical parametric amplifiers, Rev. Sci. Instrum. **74**, 1 (2003)

[10] A. Dubietis, G. Jonušauskas, and A. Piskarskas, Powerful femtosecond pulse generation by chirped and stretched pulse parametric amplification in bbo crystal, Opt. Commun. **88**, 437 (1992).

[11] I. N. Ross, P. Matousek, G. H. C. New, and K. Osvay, Analysis and optimization of optical parametric chirped pulse amplification, J. Opt. Soc. Am. B **19**, 2945 (2002).

[12] F. Théberge, N. Aközbek, W. Liu, A. Becker, and S. L. Chin, Tunable Ultrashort Laser Pulses Generated through Filamentation in Gases, Phys. Rev. Lett. **97**, 023904 (2006).

[13] T. Fuji and T. Suzuki, Generation of sub-two-cycle mid-infrared pulses by four-wave mixing through filamentation in air, Opt. Lett. **32**, 3330 (2007).

[14] M. Nisoli, S. De Silvestri, and O. Svelto, Generation of high energy 10 fs pulses by a new pulse compression technique, Appl. Phys. Lett. **68**, 2793 (1996).

[15] M. Nisoli, S. D. Silvestri, O. Svelto, R. Szipöcs, K. Ferencz, C. Spielmann, S. Sartania, and F. Krausz, Compression of high-energy laser pulses below 5 fs, Opt. Lett. **22**, 522 (1997).

[16] T. Sylvestre, E. Genier, A. N. Ghosh, P. Bowen, G. Genty, J. Troles, A. Mussot, A. C. Peacock, M. Klimczak, A. M. Heidt, J. C. Travers, O. Bang, and J. M. Dudley, Recent advances in supercontinuum generation in specialty optical fibers [invited], J. Opt. Soc. Am. B **38**, F90 (2021).

[17] A. Mussot, T. Sylvestre, L. Provino, and H. Maillotte, Generation of a broadband single-mode supercontinuum in a conventional dispersion-shifted fiber by use of a subnanosecond microchiplaser, Opt. Lett. **28**, 1820 (2003).

[18] C. Lesvigne, V. Couderc, A. Tonello, P. Leproux, A. Barthélémy, S. Lacroix, F. Druon, P. Blandin, M. Hanna, and P. Georges, Visible supercontinuum generation controlled by intermodal four-wave mixing in microstructured fiber, Opt. Lett. **32**, 2173 (2007).

[19] S. Perret, G. Fanjoux, L. Bigot, J. Fatome, G. Millot, J. M. Dudley, and T. Sylvestre, Supercontinuum generation by intermodal four-wave mixing in a step-index few-mode fibre, APL Photonics **4**, 022905 (2019).

[20] P.-A. Champert, V. Couderc, P. Leproux, S. Février, V. Tombelaine, L. Labonté, P. Roy, C. Froehly, and P. Nérin, White-light supercontinuum generation in normally dispersive optical fiber using original multi-wavelength pumping system, Opt. Express **12**, 4366 (2004).

[21] W. J. Wadsworth, N. Joly, J. C. Knight, T. A. Birks, F. Biancalana, and P. S. J. Russell, Supercontinuum and four-wave mixing with q-switched pulses in endlessly single-mode photonic crystal fibres, Opt. Express **12**, 299 (2004).

[22] R. Dupiol, A. Bendahmane, K. Krupa, A. Tonello, M. Fabert, B. Kibler, T. Sylvestre, A. Barthelemy, V. Couderc, S. Wabnitz, and G. Millot, Far-detuned cascaded intermodal four-wave mixing in a multimode fiber, Opt. Lett. **42**, 1293 (2017).

[23] R. Safaei, G. Fan, O. Kwon, K. Légaré, P. Lassonde, B. E. Schmidt, H. Ibrahim, and F. Légaré, High-energy multidimensional solitary states in hollow-core fibres, Nat. Photon. **14**, 733 (2020).

[24] J. E. Beetar, M. Nrisimhamurty, T.-C. Truong, G. C. Nagar, Y. Liu, J. Nesper, O. Suarez, F. Rivas, Y. Wu, B. Shim, and M. Chini, Multioctave supercontinuum generation and frequency conversion based on rotational nonlinearity, Sci. Adv. **6**, eabb5375 (2020).

[25] G. Fan, R. Safaei, O. Kwon, V. Schuster, K. Légaré, P. Lassonde, A. Ehteshami, L. Arias, A. Laramée, J. Beaudoin-Bertrand, J. Limpert, Z. Tao, M. Spanner, B. E. Schmidt, H. Ibrahim, A. Baltuška, and F. Légaré, High energy redshifted and enhanced spectral broadening by molecular alignment, Opt. Lett. **45**, 3013 (2020).

[26] P. A. Carpeggiani, G. Coccia, G. Fan, E. Kaksis, A. Pugžlys, A. Baltuška, R. Piccoli, Y.-G. Jeong, A. Rovere, R. Morandotti, L. Razzari, B. E. Schmidt, A. A. Voronin, and A. M. Zheltikov, Extreme raman red shift: Ultrafast multimode nonlinear space-time dynamics, pulse compression, and broadly tunable frequency conversion, Optica **7**, 1349 (2020).

[27] J. Wu, H. Cai, Y. Peng, Y. Tong, A. Couairon, and H. Zeng, Control of femtosecond filamentation by field-free revivals of molecular alignment, Laser Phys. **19**, 1759 (2009).

[28] J. Wu, H. Cai, H. Zeng, and A. Couairon, Femtosecond filamentation and pulse compression in the wake of molecular alignment, Opt. Lett. **33**, 2593 (2008).

[29] J. Wu, H. Cai, A. Couairon, and H. Zeng, Wavelength tuning of a few-cycle laser pulse by molecular alignment in femtosecond filamentation wake, Phys. Rev. A **79**, 063812 (2009).

[30] J. Wu, H. Cai, Y. Peng, and H. Zeng, Controllable supercontinuum generation by the quantum wake of molecular alignment, Phys. Rev. A **79**, 041404(R) (2009).

[31] H. Cai, J. Wu, Y. Peng, and H. Zeng, Comparison study of supercontinuum generation by molecular alignment of n2 and o2, Opt. Express **17**, 5822 (2009).

[32] Y. Huang, C. Meng, X. Wang, Z. Lü, D. Zhang, W. Chen, J. Zhao, J. Yuan, and Z. Zhao, Joint Measurements of Terahertz Wave Generation and High-Harmonic Generation from Aligned Nitrogen Molecules Reveal Angle-Resolved Molecular Structures, Phys. Rev. Lett. **115**, 123002 (2015).

[33] Y. Liu, A. Houard, B. Prade, S. Akturk, A. Mysyrowicz, and V. T. Tikhonchuk, Terahertz Radiation Source in Air Based on Bifilamentation of Femtosecond Laser Pulses, Phys. Rev. Lett. **99**, 135002 (2007).

[34] M. Durand, Y. Liu, A. Houard, and A. Mysyrowicz, Fine control of terahertz radiation from filamentation by molecular lensing in air, Opt. Lett. **35**, 1710 (2010).

[35] D. J. Cook and R. M. Hochstrasser, Intense terahertz pulses by four-wave rectification in air, Opt. Lett. **25**, 1210 (2000).

[36] J. Wu, Y. Tong, M. Li, H. Pan, and H. Zeng, Thz generation by a two-color pulse in prealigned molecules, Phys. Rev. A **82**, 053416 (2010).

[37] R. Velotta, N. Hay, M. B. Mason, M. Castillejo, and J. P. Marangos, High-Order Harmonic Generation in Aligned Molecules, Phys. Rev. Lett. **87**, 183901 (2001).

[38] N. Hay, R. Velotta, M. Lein, R. de Nalda, E. Heesel, M. Castillejo, and J. P. Marangos, High-order harmonic generation in laser-aligned molecules, Phys. Rev. A **65**, 053805 (2002).

[39] V. Kalosha, M. Spanner, J. Herrmann, and M. Ivanov, Generation of Single Dispersion Precompensated 1-fs Pulses by Shaped-Pulse Optimized High-Order Stimulated Raman Scattering, Phys. Rev. Lett. **88**, 103901 (2002).

[40] F. Zhong, H. Jiang, and Q. Gong, Generation of intense frequency-tunable few-cycle femtosecond pulses in hollow fiber, J. Opt. Soc. Am. B **27**, 128 (2010).

[41] F. Wang, H. Jiang, and Q. Gong, Frequency tuning enhancement of few-cycle femtosecond laser pulses by double-pump-induced n2 index modulation, J. Opt. Soc. Am. B **29**, 232 (2012).

[42] F. Zhong, H. Jiang, and Q. Gong, Tuning the frequency of few-cycle femtosecond laser pulses by molecular phase modulation, Opt. Express **17**, 1472 (2009).

[43] N. Zhavoronkov and G. Korn, Generation of Single Intense Short Optical Pulses by Ultrafast Molecular Phase Modulation, Phys. Rev. Lett. **88**, 203901 (2002).

[44] R. A. Bartels, T. C. Weinacht, N. Wagner, M. Baertschy, C. H. Greene, M. M. Murnane, and H. C. Kapteyn, Phase Modulation of Ultrashort Light Pulses using Molecular Rotational Wave Packets, Phys. Rev. Lett. **88**, 013903 (2001).

[45] F. Noack, O. Steinkellner, P. Tzankov, H.-H. Ritze, J. Herrmann, and Y. Kida, Generation of sub-30 fs ultraviolet pulses by raman induced phase modulation in nitrogen, Opt. Express **13**, 2467 (2005).

[46] A. Nazarkin, G. Korn, M. Wittmann, and T. Elsaesser, Group-velocity-matched interactions in hollow waveguides: Enhanced high-order raman scattering by impulsively excited molecular vibrations, Phys. Rev. A **65**, 041802(R) (2002).

[47] S. Baker, I. A. Walmsley, J. W. G. Tisch, and J. P. Marangos, Femtosecond to attosecond light pulses from a molecular modulator, Nat. Photon. **5**, 664 (2011).

[48] H. Cai, J. Wu, X. Bai, H. Pan, and H. Zeng, Molecular-alignment-assisted high-energy supercontinuum pulse generation in air, Opt. Lett. **35**, 49 (2010).

[49] H. Cai, J. Wu, A. Couairon, and H. Zeng, Spectral modulation of femtosecond laser pulse induced by molecular alignment revivals, Opt. Lett. **34**, 827 (2009).

[50] F. Calegari, C. Vozzi, S. Gasilov, E. Benedetti, G. Sansone, M. Nisoli, S. De Silvestri, and S. Stagira, Erratum: Rotational Raman Effects in the Wake of Optical Filamentation [Phys. Rev. Lett. **100**, 123006 (2008)], Phys. Rev. Lett. **101**, 179902(E) (2008).

[51] F. Calegari, C. Vozzi, S. Gasilov, E. Benedetti, G. Sansone, M. Nisoli, S. De Silvestri, and S. Stagira, Rotational Raman Effects in the Wake of Optical Filamentation, Phys. Rev. Lett. **100**, 123006 (2008).

[52] Z. Huang, D. Wang, Y. Leng, and Y. Dai, Tuning the central wavelength by hundreds of nanometers using ultrafast molecular phase modulation, Phys. Rev. A **91**, 043809 (2015).

[53] Y.-H. Chen, S. Varma, A. York, and H. M. Milchberg, Single-shot, space- and time-resolved measurement of rotational wavepacket revivals in h2, d2, n2, o2, and n2o, Opt. Express **15**, 11341 (2007).

[54] P. Béjot, B. E. Schmidt, J. Kasparian, J.-P. Wolf, and F. Legaré, Mechanism of hollow-core-fiber infrared-supercontinuum compression with bulk material, Phys. Rev. A **81**, 063828 (2010).

[55] B. Lavorel, P. Babilotte, G. Karras, F. Billard, E. Hertz, and O. Faucher, Measurement of dichroism in aligned molecules, Phys. Rev. A **94**, 043422 (2016).

[56] S. Mukamel, *Principles of Nonlinear Optical Spectroscopy* (Oxford University Press, New York, 1995).

[57] A. Couairon and A. Mysyrowicz, Femtosecond filamentation in transparent media, Phys. Rep. **441**, 47 (2007).

[58] M. Nurhuda, A. Suda, K. Midorikawa, M. Hatayama, and K. Nagasaka, Propagation dynamics of femtosecond laser pulses in a hollow fiber filled with argon: Constant gas pressure versus differential gas pressure, J. Opt. Soc. Am. B **20**, 2002 (2003).

[59] N. Kaya, G. Kaya, M. Sayrac, Y. Boran, S. Anumula, J. Strohaber, A. A. Kolomenskii, and H. A. Schuessler, Probing nonadiabatic molecular alignment by spectral modulation, Opt. Express **24**, 2562 (2016).

[60] J. Ortigoso, M. Rodriguez, M. Gupta, and B. Friedrich, Time evolution of pendular states created by the interaction of molecular polarizability with a pulsed nonresonant laser field, J. Chem. Phys. **110**, 3870 (1999).